Am J Physiol Heart Circ Physiol 319: H882–H892, 2020.
First published August 21, 2020; doi:10.1152/ajpheart.00172.2020.

RESEARCH ARTICLE | *Integrative Cardiovascular Physiology and Pathophysiology*

Biomechanics of diastolic dysfunction: a one-dimensional computational modeling approach

Karim Kadry,[1] Stamatia Pagoulatou,[1] Quentin Mercier,[1] Georgios Rovas,[1] Vasiliki Bikia,[1] Hajo Müller,[2] Dionysios Adamopoulos,[2] and Nikolaos Stergiopulos[1]

[1]*Laboratory of Hemodynamics and Cardiovascular Technology, Ecole Polytechnique Fédérale de Lausanne, Lausanne, Switzerland.; and* [2]*Department of Cardiology, Hôpitaux Universitaires de Genève, Geneva, Switzerland*

Submitted 11 March 2020; accepted in final form 19 August 2020

Kadry K, Pagoulatou S, Mercier Q, Rovas G, Bikia V, Müller H, Adamopoulos D, Stergiopulos N. Biomechanics of diastolic dysfunction: a one-dimensional computational modeling approach. *Am J Physiol Heart Circ Physiol* 319: H882–H892, 2020. First published August 21, 2020; doi:10.1152/ajpheart.00172.2020.—Diastolic dysfunction (DD) is a major component of heart failure with preserved ejection fraction (HFpEF). Accordingly, a profound understanding of the underlying biomechanical mechanisms involved in DD is needed to elucidate all aspects of HFpEF. In this study, we have developed a computational model of DD by leveraging the power of an advanced one-dimensional arterial network coupled to a four-chambered zero-dimensional cardiac model. The two main pathologies investigated were linked to the active relaxation of the myocardium and the passive stiffness of the left ventricular wall. These pathologies were quantified through two parameters for the biphasic delay of active relaxation, which simulate the early and late-phase relaxation delay, and one parameter for passive stiffness, which simulates the increased nonlinear stiffness of the ventricular wall. A parameter sensitivity analysis was conducted on each of the three parameters to investigate their effect in isolation. The three parameters were then concurrently adjusted to produce the three main phenotypes of DD. It was found that the impaired relaxation phenotype can be replicated by mainly manipulating the active relaxation, the pseudo-normal phenotype was replicated by manipulating both the active relaxation and passive stiffness, and, finally, the restricted phenotype was replicated by mainly changing the passive stiffness. This article presents a simple model producing a holistic and comprehensive replication of the main DD phenotypes and presents novel biomechanical insights on how key parameters defining the relaxation and stiffness properties of the myocardium affect the development and manifestation of DD.

NEW & NOTEWORTHY This study uses a complete and validated computational model of the cardiovascular system to simulate the two main pathologies involved in diastolic dysfunction (DD), i.e., abnormal active relaxation and increased ventricular diastolic stiffness. The three phenotypes of DD were successfully replicated according to literature data. We elucidate the biomechanical effect of the relaxation pathologies involved and how these pathologies interact to create the various phenotypes of DD.

active relaxation; biphasic delay; diastolic dysfunction; diastolic left ventricular stiffness; heart failure with preserved ejection fraction

INTRODUCTION

Heart failure (HF) is a cardiac disease that currently affects 2% of the population (18). Originally, HF was attributed to left ventricular (LV) systolic dysfunction, as reflected by a reduced ejection fraction (HFrEF). However, it is now recognized that nearly half or more of patients with HF have a preserved ejection fraction (HFpEF) but manifest some degree of dysfunction during the diastolic period of the cardiac cycle. Although both HF types contribute equally to the high morbidity and mortality rates, the prevalence of HFpEF has an increasing trend (45). This is primarily due to a poor understanding of the disease mechanisms and the increasing population age. One of the main diagnostic criteria for HFpEF is evidence of left ventricular diastolic dysfunction (DD) (33). Therefore, a good understanding of the main physiological mechanisms behind diastolic dysfunction is needed to gain a more comprehensive picture of HFpEF.

The diastolic portion of the cardiac cycle is controlled by two main factors: the active relaxation of the myocardium and the passive mechanical properties of the ventricular wall. Active relaxation is characterized by the pressure decay time constant τ and passive mechanical properties by diastolic stiffness. The various stages of DD have been understood to result from some combination of delayed and incomplete active relaxation of the ventricle and increased ventricular stiffness, independent of the presence of a normal or reduced ejection fraction (51). However, isolating the exact effects of impaired active relaxation and increased ventricular stiffness has proved to be a challenge owing to the inherent biological and biomechanical interactions of the underlying mechanisms. Accordingly, the diagnosis of diastolic dysfunction is conducted by measuring various cardiovascular parameters. In clinical practice, invasively determined diastolic pressures are used as a surrogate of diastolic function. However, it must be noted that this is not considered the sole gold standard for diastolic function analysis, as various other indexes are used in conjunction for diagnosis.

The hemodynamics of the atrioventricular system in diastole can be split into two main phases. The first is the early relaxation (*E*) phase in which the ventricles rapidly relax and fill up with blood. In healthy subjects, this phase contributes to ~85% of the ejected blood volume in the ventricles. Afterward, more blood is forced into the ventricles during the atrial contraction (*A*) phase. The presence and progression of diastolic dysfunction has been known to affect the relationship

Correspondence: S. Pagoulatou (stamatia.pagoulatou@epfl.ch).

between *E* and *A* flows at the level of the mitral valve and is associated with an increase in left ventricular and atrial pressures.

The most common diagnostic method for diastolic dysfunction is the use of echocardiography owing to its noninvasive nature. Numerous Doppler indexes are used to describe diastolic function and refer to different filling phases and pressure levels. This contributes to the inconsistencies that are sometimes observed in prediction of LV filling pressure between the different indexes. Typically, the measurement of the peak mitral flow velocity of both diastolic phases, along with a measure of the flow deceleration (deceleration time or DT) (51) and the mitral annulus velocities, is performed. The formal diagnostic algorithm also includes left atrium enlargement as a surrogate for chronic elevated left-side filling pressures and signs of pulmonary hypertension. There are three disease types that reflect different levels of diastolic dysfunction (51). The impaired relaxation (IR) type is characterized by a decreased ratio between the peak *E* phase mitral flow and peak A phase mitral flow (*E*/*A* ratio) and by a long deceleration time and normal end-diastolic pressure. The pseudo-normal (PN) type is characterized by a normal-seeming *E*/*A* ratio, normal deceleration time, and elevated end-diastolic pressure. Finally, the restricted (R) type is characterized by a very high *E*/*A* ratio, short deceleration time, and highly elevated end-diastolic pressure. The PN phenotype of diastolic dysfunction creates much ambiguity in terms of diagnosis, as the mitral flow mimics normal flow and other indexes have to be integrated for the correct diagnosis. However, this diagnostic algorithm cannot be applied to certain subgroups of patients, e.g., conduction delay, pacemaker stimulation, atrial fibrillation, and mitral valve disease. Echocardiographic analysis is furthermore complicated by age and loading condition dependency of the parameters, but in most patients, at least one parameter is abnormal (52).

It is important to note that the pathologies regarding HFpEF are not restricted to just left ventricular diastolic dysfunction. Longitudinal strain is reduced in HFpEF, and two-dimensional (2-D) speckle-tracking echocardiography has proven to be robust and useful to detect this condition (47). The contractility (in terms of end-systolic elastance) of the left ventricle during systole has been shown to increase in patients with HFpEF, although the degree varies from study to study (3, 16, 19, 34). Recent studies have shown that the right ventricle also tends to exhibit structural and functional changes in patients with HFpEF (24, 39, 46). The left atrium has been shown to undergo remodeling in diastolic dysfunction, likely due to the increased pressures (8, 30, 44). With regard to systemic vascular remodeling, multiple studies have shown that vascular resistance (16, 19) and vascular stiffness (3, 16, 19) are raised in HFpEF. Consequently, it is currently understood that HFpEF is a highly heterogeneous disorder of which diastolic dysfunction is only a component. It is also possible to have diastolic dysfunction without HFpEF, as is the case in aging and diabetic populations (49). Accordingly, there is a need for robust computational models that can investigate the relation between the biomechanical effects of diastolic dysfunction and other comorbidities listed previously such as arterial hypertension, arterial stiffening, chamber remodeling, arrhythmia, valve dysfunction, and exercise. Furthermore, the creation of a complete computational model may allow for the development of novel diagnostic tools and therapeutic strategies for these patients, as no efficacious treatment has been developed to date.

The current state of computational modeling of diastolic dysfunction is still in its infancy. A computational model by Hay et al. (12) investigated the effect of increasing ventricular relaxation time and its effect on cardiac output and pulmonary vein pressure for different heart rates. The fundamental insight from this work is that a delay applied for LV relaxation during early diastolic filling is able to replicate the characteristic mitral waveform associated with impaired relaxation. However, as the delay was only applied after isovolumic relaxation had ended, they were unable to replicate other aspects of the disease related to contraction and isovolumic relaxation, such as time constant of relaxation and prolonged ejection, which are markedly increased in DD (14, 48). Luo et al. (23) also used a zero-dimensional (0-D) model of the cardiovascular system to replicate some phenotypic aspects of impaired relaxation, pseudo-normal, and restricted phenotypes by manipulating the active relaxation and passive properties of the heart. The fundamental insight gained is that increased stiffness shifts the mitral waveform toward that of restricted diastolic dysfunction. However, the impaired relaxation phenotype produced was created such that end-diastolic pressure (EDP) was significantly increased, a finding not supported by the clinical literature (14). Furthermore, the stroke volumes were significantly decreased for all three phenotypes, another finding not consistent with the literature (6, 44). Finally, the pseudo-normal phenotype was created through directly combining the impaired relaxation and restricted phenotypes, which produced a phenotype that was higher in EDP than that of the restricted, a finding that is not supported by the current literature (13).

In contrast to these approaches, we aimed at the development of a computational model of diastolic dysfunction that also incorporates the insights gained from previous literature and includes the interaction of the left ventricle with the arterial system. It consists of an already existing and validated model of the arterial tree coupled to an upgraded four-chamber lumped parameter model of the heart including valve dynamics. The main novelty in this article is the implementation of a biphasic delay mechanism, which consists of early and late-phase delays. This biphasic delay mechanism was then used along with increased hyperelastic chamber stiffness and venous pressure on this computational platform to holistically investigate the pathological mechanisms of the different stages of diastolic dysfunction.

MATERIALS AND METHODS

The Cardiovascular Model

The open-loop one-dimensional (1-D) model of the arterial tree was previously developed (37) and validated (36) in our laboratory. Originally, the arterial tree model by Reymond et al. (37) was coupled at its proximal end to a 0-D model of the left ventricle of the heart, in which the temporal pressure-volume (PV) relationship is inputted manually through a time-varying elastance curve (41). In this work, the cardiac model was upgraded to include all four chambers of the heart and to better capture the valve dynamics. The left and right atria are coupled together using a pulmonary lumped parameter model, and a central venous pressure boundary condition is connected to the right atrium with a resistance in between. This improvement is largely inspired by the work of Mynard et al. (27, 28). The ventricular chambers also had their pressures coupled

through a septal interaction relation. The contractility of each chamber was modeled by distinct time-varying elastance functions. To account for the pressure loss observed during the nonisovolumic contraction, a source resistance was introduced into the model to yield the effective elastance, as done by Reymond et al. (37). Finally, the pulmonary circulation was described with a five-segment lumped parameter model (2-element Windkessel models connected in series), as in the work of Danielsen et al. (7). An in-depth description of the model along with all the parameters used can be found in the supplementary information (all Supplemental material is available at https://doi.org/10.6084/m9.figshare.12661901.v1).

The Upgraded Pressure-Volume Relation

In the original model, the LV pressure-volume relation was considered linear throughout the cardiac cycle. Although this assumption has been seen to hold for healthy hearts and many cardiac pathologies, one key feature of diastolic dysfunction is the increase in nonlinearity of the LV end-diastolic pressure-volume relation (EDPVR), and thus, the linear assumption was relaxed to fully capture the later stages of the pathology. Ignoring the nonlinearity of the LV EDPVR when modeling diastolic dysfunction would severely hamper our ability to faithfully capture the disease hemodynamic characteristics (cf. DISCUSSION). Accordingly, a segregated version of the pressure-volume relation, similar to that of Luo et al. (23), was used for the left ventricle, in which the free wall pressure-volume relation P_{LVF} is an addition of a linear systolic pressure-volume relation P_s and a nonlinear diastolic pressure-volume relation P_d. The contraction of the heart was controlled by a time-varying activation function $\varepsilon(t)$, which controls the weight that each term adds to the total pressure-volume relation. The LV end-diastolic pressure-volume relation was modeled as an exponential function where P_0 is the dead pressure and β is the stiffness parameter. It is important to note that when β is small, the exponential function approximates a linear curve.

$$P_{LVF} = \varepsilon(t) \cdot P_s + \left[1 - \varepsilon(t)\right] \cdot P_d \quad (1)$$

where

$$P_s = E_{max} \cdot \left(V_{LV} - V_d\right) \quad (2)$$

and

$$P_d = P_0 \cdot \exp\left(\beta \cdot V_{LV}\right) \quad (3)$$

E_{max} is the maximal elastance and V_d is the dead volume, as described by Sagawa (40). The free wall pressure is then corrected for septal interaction and pressure loss during ejection according to the aortic flow rate. Details on how this was done are contained in the online appendix.

Diastolic Dysfunction Parameters: Biphasic Delay for Active Relaxation

After systole, the lengthening of the ventricular myocardium is mediated by the active removal of calcium ions. This lengthening occurs during both the isovolumic (through untwisting) and filling (through expansion) phases of relaxation. Inadequate relaxation has been implicated in diastolic dysfunction, mainly owing to calcium mishandling and increased myofilament calcium sensitivity (10, 51). To model the effect of inadequate active relaxation, the diastolic portion of the activation function underwent specific shape changes corresponding to either the early or the late phase of diastolic relaxation. The early phase of relaxation is related to the isovolumic part of the diastole, whereas the late phase of relaxation is assumed to be related to the filling phase of diastole.

To model the impaired relaxation at the early phase of relaxation, the portion of the activation function $\varepsilon(t)$ after the systolic peak was made to undergo a horizontal stretching proportional to the distance to the peak (Fig. 1*A*). The degree of this early phase delay was controlled by the parameter D_1, which was limited such that the curve still had to return to a value of 0 before the heart cycle ended. To model the impaired relaxation at the late phase of relaxation, the portion of the curve at the tail end of the activation function was made to undergo a similar transformation (Fig. 1*B*). The degree of the late-phase delay was controlled by the parameter D_2.

Diastolic Dysfunction Parameters: Passive Relaxation

The end-diastolic pressure-volume relation can be changed in two ways. The first is through changing the dead pressure P_0, which results in the vertical shift of the LV EDPVR. The second is through changing the stiffness parameter β, increasing or decreasing the instantaneous dP/dV relation at each point of the LV EDPVR, and thus changing the diastolic elastic properties of the heart (Fig. 1*C*). For the purposes of this study, only the β parameter was analyzed, as that was determined to be the most physiologically relevant.

Parameter Sensitivity Analysis

To gauge the effect of the various parameters on the hemodynamics of the model, a parameter sensitivity analysis was conducted with the parameters D_1, D_2, and β (Figs. 1 and 2). The parameters were varied in the following ranges: $D_1 \in [0, 0.7]$ mmHg, $D_2 \in [0, 0.9]$, and $\beta \in [0.011, 0.017]$ mL^{-1}. The control values of $P_0 = 2.3$ mmHg and $\beta = 0.011$ mL^{-1} for the left ventricle were obtained from the study by Zile et al. (50). Furthermore, the control activation function was set to have a time relaxation constant similar to the one reported by Zile et al. (50). To calculate the time constant of relaxation, the isovolumic pressure was modeled as an exponentially decreasing function. Accordingly, the time constant was defined as the time interval between start of isovolumic relaxation and the time at which the LV pressure dropped to 1/e of its original value. Finally, the isovolumic relaxation time (IVRT) was calculated from the aortic flow waveform.

From the simulation results, we analyzed the left ventricular and atrial PV loops and the aortic and mitral flow patterns and quantified the following hemodynamic parameters: the cardiac output, *E*-wave peak, *A*-wave peak, *E*/*A* ratio, filling pressure, maximal left atrial pressure, ejection fraction, time relaxation constant, and isovolumic relaxation time (IVRT).

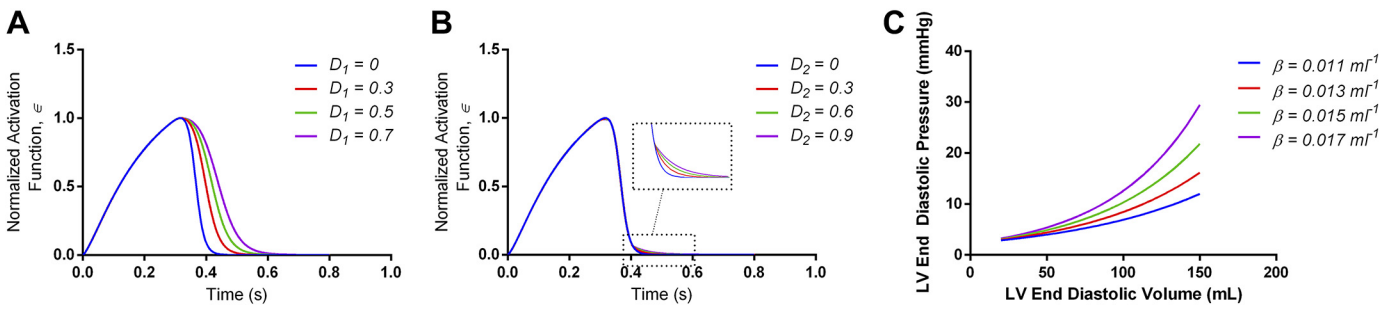

Fig. 1. Changes in the activation function $\varepsilon(t)$ and the LV EDPVR by varying three parameters: early delayed relaxation ($D1$) (*A*), late delayed relaxation ($D2$) (*B*), and stiffness parameter (β) (*C*).

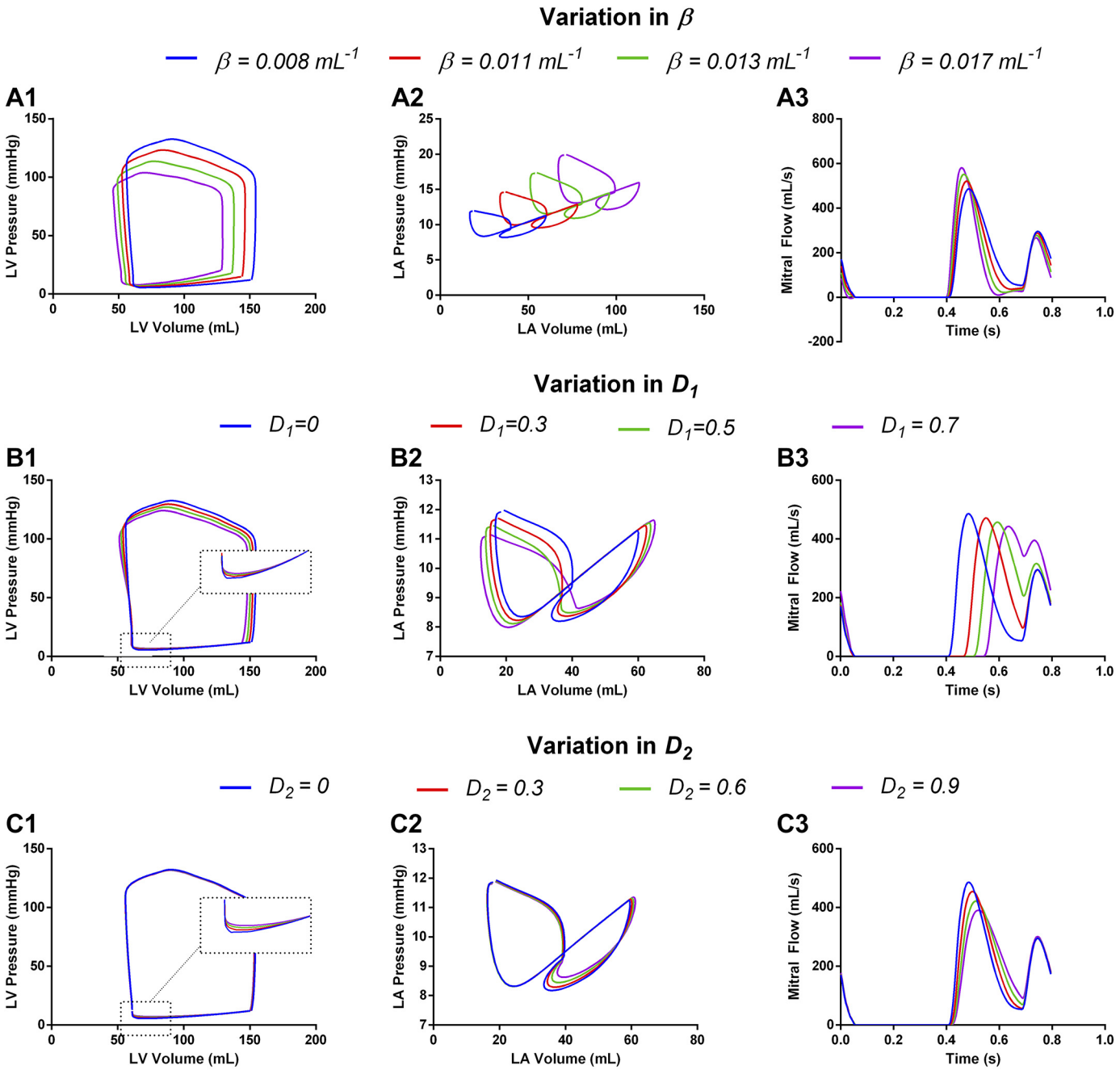

Fig. 2. Results of the parameter sensitivity analysis, which includes the left ventricular PV loops (*A1*, *B1*, and *C1*), left atrial PV loops (*A2*, *B2*, and *C2*), and mitral flow profiles (*A3*, *B3*, and *C3*), over D_1 (*B1*, *B2*, and *B3*), D_2 (*C1*, *C2*, and *C3*), and β (*A1*, *A2*, and *A3*).

Modeling the Progression of Diastolic Dysfunction

Based on the insights gained from the parameter sensitivity analysis, we replicated the IR, PN, and R mitral flow patterns by changing the three parameters discussed earlier, i.e., D_1, D_2, and β. The set of parameters used for the phenotypic replication of the disease stages is shown in Table 1. The choice of parameters was guided based on the current available literature on the *E/A* ratios, time constants, end-diastolic pressures, and cardiac outputs to allow for the replication of the expected hemodynamic parameters seen in diastolic dysfunction studies. The existence of normal end-diastlic volume (EDVs) in patients with DD implies the existence of compensatory mechanisms, such as increased contractility (i.e., end-systolic elastance), arterial stiffness, and venous pressure, to properly maintain the cardiac output and systemic pressures. Previous studies have shown that patients with HFpEF have higher LV end-systolic elastance (19, 39, 46) and an increased venous pressure (4, 15). In our work, we found that by adjusting just the cardiac preload along with varying the pathological parameters such as delay and stiffness, we were able to fully replicate the three disease phenotypes. In other words, although contractility and stiffness of the four cardiac chambers influence the analyzed parameters, the venous pressure had the strongest role in adjusting the ventricular volumes and, accordingly, was chosen as the sole additional factor to adjust. It must be stressed that a holistic replication of DD was emphasized when choosing the parameters. For example, it was possible to create a mitral waveform that has an *E/A* ratio of 2 (similar to that of R) by only increasing the central venous pressure.

Table 1. *Parameters used to replicate the three stages of the disease with pressure compensation mechanisms*

Parameter	Control	IR	PN	R
D_1	0	0.25	0.25	0.25
D_2	0	1.3	0.45	0
β, mL^{-1}	0.011	0.011	0.0145	0.016
Venous pressure, mmHg	6	6.25	7.12	7.5

IR, impaired relaxation; PN, pseudo-normal; R, restricted.

However, this would have caused the cardiac output to surpass physiological levels. The goal instead was to model the combination of fundamental pathologies that capture the various aspects of DD in terms of EDP, cardiac output, relaxation times, etc.

The general algorithm for producing each phenotype is the following. First, the early phase delay D_1 was increased until the desired time constant of relaxation is achieved. In this article, the three phenotypes were assumed to have the same time constant of relaxation that was higher than that of the control. This is in accordance to reviews (14) and a clinical study that found little difference between the time constants for each stage (43). The time constant was initially set at a control value of 40 ms, similar to that found by Zile et al. (50). The time constant was then increased to be in the range of 50–60 ms (43). It is important to note that the time resolution of the simulation was 5 ms, so the possible target values were constrained to be in multiples of 5. Once the time constant of relaxation was tuned, the remaining relevant parameters, namely, D_2, β, and central venous pressure, were varied to reproduce the expected *E*/*A* ratio and EDP, while maintaining the cardiac output. The assumption of maintained cardiac output comes from the clinical finding that no significant difference in stroke volume is found between the DD stages and controls (25, 44).

The target *E*/*A* ratio for the IR phenotype was determined to be 0.8 according to guidelines (29) and clinical studies (17, 43, 44). This *E*/*A* ratio was achieved by increasing D_2 and central venous pressure until the target ratio was reached and cardiac output was maintained. Another constraint placed on the tuning process was that the filling pressure for the IR stage is not markedly increased according to official guidelines (29) and clinical studies (13, 43). The target *E*/*A* ratio for the PN phenotype was determined to be equal to that of the control value of 1.6 according to guidelines (29) and clinical studies (25, 43, 44). The *E*/*A* ratio was achieved by increasing D_2, β, and central venous pressure while maintaining cardiac output. The filling pressure was also constrained to be within the range of 20 mmHg according to the clinical literature (13, 25, 43). The target *E*/*A* ratio for the R phenotype was set to be larger than 2 (in this case, 2.3) according to guidelines (29) and clinical studies (44). The *E*/*A* ratio was achieved by increasing βand central venous pressure while maintaining cardiac output. The filling pressure was also constrained to be within the range of 26 mmHg according to the clinical literature (13).

RESULTS

Parameter Sensitivity Analysis Results

In the following paragraphs, we describe the results from the parameter sensitivity analysis with respect to the PV loop of the left ventricle, the PV loop of the left atrium, and hemodynamic indexes. The results are summarized in Fig. 2 and Table 2.

Left ventricular pressure-volume loop. We found that because the EDPVR (P_d) is only affected by the β parameter, an increase in stiffness β caused the LV systolic pressure and stroke volume to decrease significantly (Fig. 2*A1*). Accordingly, an increase in β caused the LV diastolic pressure to rise rapidly with increasing volume. This means that given the same central venous preload, the ventricle pressure should equalize with the atrial pressure during diastole at a smaller volume. Increasing D_1 prolonged the ejection phase and increased ejection time; this can be seen by noticing the decrease in minimum volume of the PV loops with increasing D_1 in Fig. 2*B1*. Correspondingly, the prolongation of both contraction and relaxation through D_1 decreased the EDV and EDP to a small degree. One notable effect is that an increase in D_1 disallowed the activation function in early diastole to reach 0, which is what would occur if relaxation was normal. This means that the pressure-volume relation is the sum of a large fraction (inversely proportional to the nonzero activation level) of the EDPVR (P_d) and a small fraction (proportional to the nonzero activation level) of the ESPVR (P_s). This can be seen by examining the zoomed-in view of early diastole in Fig. 2*B1*, where the control PV loop dropped to follow the exponential EDPVR (thus acting as a purely passive stiff vessel) at low volumes, whereas the delayed relaxation PV loops converged to the same EDPVR at different rates. A change in the D_2 also slowed the rate of LV pressure drop during early diastole and prevented the LV from acting as a purely stiff vessel (as the activation function is nonzero). This can be seen by examining the zoomed-in view of Fig. 2*C1*, where increasing the delay parameter increased the volume at which the PV loop follows a purely exponential EDPVR. As expected, we find that changing D_2 did not affect any of the end-systolic or end-diastolic pressures and volumes (Fig. 2*C1*). This can be explained by the fact that the late-phase delay is applied after the contraction phase is over.

Table 2. *Hemodynamic indexes of parameter sensitivity analysis*

	Value of D_1				Value of D_2				Value of β (10^{-3} mL^{-1})			
Hemodynamic indexes	0	0.3	0.5	0.7	0	0.3	0.6	0.9	11	13	15	17
Cardiac output, L/min	5.6	5.49	5.39	5.28	5.59	5.58	5.58	5.56	5.6	5.29	4.96	4.63
E-wave peak, mL/s	486	472	457	443	484	454	421	391	486	521	552	581
A-wave peak, mL/s	295	295	316	395	295	295	296	301	296	287	278	267
E/*A* ratio	1.64	1.60	1.45	1.12	1.64	1.54	1.42	1.30	1.64	1.81	1.98	2.17
Filling pressure, mmHg	12.1	11.8	11.5	11.1	12.0	12.0	12.0	12.0	12.1	14.8	17.7	20.3
Maximum aortic pressure, mmHg	132	129	126	123	131	131	131	131	132	122	113	104
Minimum aortic pressure, mmHg	83	81	80	78	83	83	82	82	83	78	74	70
Maximum left atrial pressure, mmHg	12.0	11.7	11.5	11.6	11.9	11.9	11.9	11.9	12	14.7	17.4	19.9
Ejection fraction, %	64%	65%	65%	66%	64%	64%	64%	64%	64%	64%	64%	65%
Isovolumic relaxation time, ms	65	110	135	160	65	70	70	75	65	65	60	55
Time relaxation constant, ms	40	65	80	100	40	40	40	40	40	40	45	40

Left atrial pressure-volume loop. For the left atrium, we found that increasing the stiffness parameter β caused a significant diagonal shift of the atrial loop along the EDPVR corresponding to an increase in atrial pressure (Fig. 2*A2*). Furthermore, an increase in stiffness changed the ratio between the atrial pump function (the atrial volume change during atrial contraction) and conduit function (the atrial volume change during early diastolic filling). This is also reflected by the increase in the *E*/*A* ratio seen in Table 2. Increasing D_1 changed the atrial loop such that maximum and minimum pressures decreased slightly (Fig. 2*B2*); furthermore, the maximum and minimum volumes increased and decreased, respectively, with D_1. Increasing D_2 only affected the PV loop such that the conduit function steadily decreased (Fig. 2, *B2* and *C2*).

Hemodynamic parameters and mitral and aortic flow patterns. We see that the *E*/*A* ratio increased significantly with increased stiffness, mainly by strongly increasing the *E*-wave peak and slightly decreasing the *A*-wave peak (Fig. 2*A3*). This also caused the cardiac output to decrease significantly in the absence of compensation mechanisms. It can also be seen that the IVRT, EF, and time relaxation constant did not change significantly with increasing stiffness. With regard to the delay parameters $D_1$and D_2, an increase in both delay parameters caused a slight decrease in cardiac output and *E*/*A* ratios. There are two mechanisms at play that change the mitral waveform with increasing D_1; the first is that the atrioventricular pressure gradient decreases slower in time due to the delay, and the second is that ejection time is prolonged, which has an effect on cardiac output and correspondingly the mitral flow (Fig. 2*B3*). The D_2 parameter only decreased the *E*-wave by keeping the LV pressure slightly higher during early diastole (Fig. 2*C3*), thus creating a smaller atrioventricular pressure gradient. Accordingly, the cardiac output was nearly unchanged with increases in either delay parameter. As expected, it can be seen that D_2 had no effect on the IVRT and time constant, whereas an increase in D_1 strongly increased both parameters. This is because D_2 only acts to delay relaxation at a later stage, after the isovolumic phase of the cardiac cycle has ended.

Diastolic Dysfunction Phenotype Results

The three disease phenotypes produced by the model and the healthy control are shown in Fig. 3, and the respective hemodynamic parameters are summarized in Table 3. A zoomed-in view of the diastolic pressure evolution for the left atrium (LA) and LV is shown in the boxes in Fig. 3.

By looking at Table 3 and Fig. 3, we observe that the IR and control LV pressure waveforms during diastole (zoomed-in view) differ in the following respect: the IR phenotype initially exhibited a higher pressure during early diastolic filling (Fig. 3, *A1* and *B1*) due to delayed relaxation. Once the LV began to expand, the control LV pressure increased quickly with increasing volume, and thus, the atrioventricular pressure was equalized at an earlier point than the IR case (Fig. 3, *A1* and *B1*). The *E*/*A* ratio for the IR phenotype is smaller than the control due to the late-phase delay causing a small atrioventricular gradient that lasts for an extended amount of time (Fig. 3*B1*). During late diastole, the pressures in the left ventricle for both the control and the IR phenotype were equal to ~12–13 mmHg, as they were completely relaxed in terms of active relaxation and acted as passively stiff chambers. As the *E*-wave does not decrease to 0 before the *A*-wave begins, the deceleration time was calculated by finding the equation of a straight line between the peak of the *E*-wave and the start of the *A*-wave. Accordingly, the IR deceleration time (DT) was found to be an elevated 340 ms (Table 3), which fits the criterion for diagnosis (>220 ms) according to guidelines and reviews (11, 14, 26). The IVRT for the IR phenotype was found to be 95 ms (Table 3), which is expected according to the standards for diagnosis (>90 ms) (11, 14).

The control and PN LV diastolic pressures (Fig. 3, *A1* and *C1*) followed similar paths. The combination of late-phase delay (which decreases the atrioventricular gradient and delays the equalization) and increased stiffness (which has the opposite effect on the gradient) allowed for the pseudo-normalization of the mitral waveform. During atrial contraction, LV pressure rapidly increased as the chamber expanded due to the increased stiffness parameter until the end-diastolic pressure of 21 mmHg was reached (Fig. 3*C1*). The mitral waveform for the PN closely mimicked that of the control (Fig. 3, *A2* and *C2*), as they both had the same *E*/*A* ratio of 1.6 and very similar deceleration times, namely, 164 ms for PN and 158 ms for control (Table 3). The finding that the DTs were roughly equal is well supported by the guidelines for diagnosis (11, 14) and clinical studies (25). Furthermore, the IVRT for both the control and the PN phenotype was found to be 65 ms and 85 ms, respectively (Table 3), in line with the current diagnostic standards (<90 ms) according to guidelines (14). It must be noted that the PN mitral wave began later than the control wave due to the isovolumic delay imposed by parameter D_1 (Fig. 3, *A2* and *C2*).

The control and R phenotype LV diastolic pressures (Fig. 3, *A1* and *D1*) dropped to similar levels during early filling; however, due to the increased LA pressure in the R phenotype, the corresponding pressure gradient was large, which led to a high *E*-wave. The increased nonlinear stiffness of the R case allowed for the LV pressure to rise rapidly with increasing volume, equalizing the atrioventricular gradient faster than the control. This increased stiffness also resulted in the LV pressure rapidly increasing during atrial contraction until it reached an end-diastolic pressure of 25 mmHg (Fig. 3, *C1* and *D1*). Accordingly, the *E*/*A* ratio for the R phenotype was the highest with a value of 2.3, and the deceleration time was the lowest with a value of 120 ms (Table 3). The DT was calculated at 120 ms (Table 3), which is within the diagnostic standards (<150 ms) provided by the guidelines (14, 29). The IVRT was calculated at 85 ms (Table 3), which is higher than what is suggested by the guidelines (<70 ms) (14). Finally, the ejection fraction managed to remain constant throughout all phenotypes at a value of ~65% (Table 3), which is supported by the clinical finding of ~60% for all stages of DD (44).

DISCUSSION

In the present study, we investigated the development and progression mechanisms of diastolic dysfunction. Our computational approach was based on an already validated, complete model of the cardiovascular system, which so far has provided a solid platform for the understanding of physiological processes such as aging (31), development of noninvasive methods to derive central hemodynamic indexes (32), and investigation of the hemodynamics of diseases such as hypertension

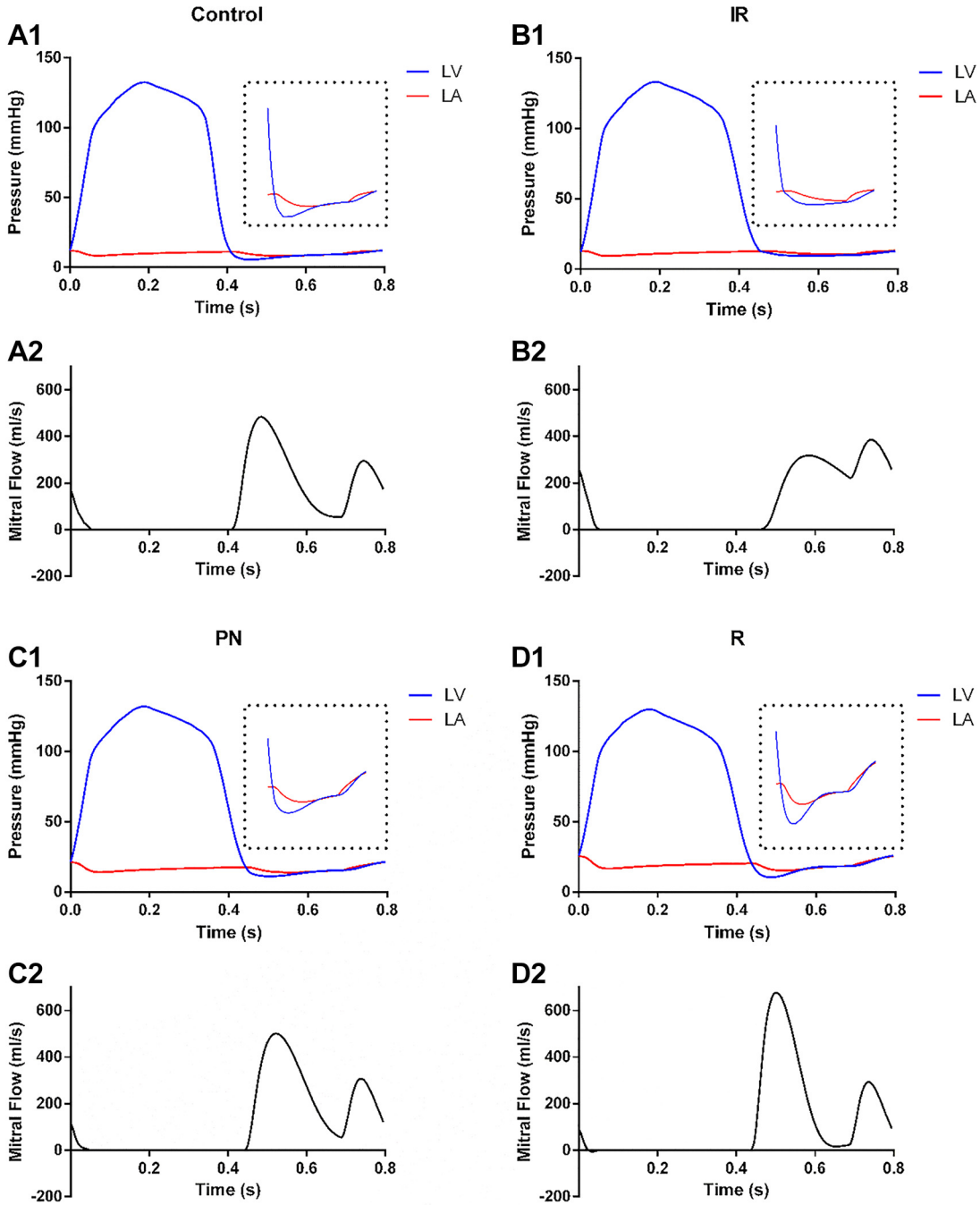

Fig. 3. Time-pressure graphs (*A1*, *B1*, *C1*, and *D1*) along with corresponding mitral flow (*A2*, *B2*, *C2*, and *D2*) for the control case (*A1* and *A2*), the IR case (*B1* and *B2*), the PN case (*C1* and *C2*), and the R case (*D1* and *D2*).

(38). There is also a strong association of DD with increasing age (43). Accordingly, the eventual goal of the model is to act as a computational platform upon which the effects of aging and hypertension can be simulated in tandem with diastolic dysfunction to investigate their effects. Our work expanded on previous studies that model diastolic dysfunction by leveraging the potential of this valuable computational tool and by following the literature data on disease initiation and progression.

The current paradigm put forward in our study is that diastolic dysfunction arises and evolves from the interplay of two principal pathologies. The first pathology is the impairment of active relaxation (represented by the activation function) where the early diastolic filling of the ventricle is altered. In most of the literature investigating impaired active relaxation, the pathology is characterized by a single time constant of relaxation related to the isovolumic phase of the cardiac cycle. This work is taking the first steps to investigate in greater detail how the time-varying rate of the active relaxation affects the hemodynamics of the left ventricle. The principal insight gained from the simulations is that a constant delay applied uniformly at the start of relaxation is unable to fully capture the IR phenotype; although the applied early delay

Table 3. *Hemodynamic indexes for each simulated phenotype*

Hemodynamic indexes	Phenotypes			
	Control	IR	PN	R
Cardiac output, L/min	5.59	5.61	5.62	5.55
E-wave peak, mL/s	484	318	500	676
A-wave peak, mL/s	295	385	306	294
E/*A* ratio	1.64	0.82	1.63	2.3
Filling pressure, mmHg	12.0	12.8	21.5	25.9
Max aortic pressure, mmHg	131	132	131	129
Min aortic pressure, mmHg	83	82	82	81
Maximum left atrial pressure, mmHg	11.9	13.0	21.2	25.5
Ejection fraction, %	64	65	65	65
Isovolumic relaxation time, ms	65	95	85	85
Time relaxation constant, ms	40	55	60	60
Deceleration time, ms	158	340	164	120

IR, impaired relaxation; PN, pseudo-normal; R, restricted.

managed to increase the time constant of relaxation, it was unable to replicate the characteristic mitral flow associated with IR. What was found to be required was a comparatively pronounced delay in the late phase of relaxation corresponding to diastolic filling. This combination of early phase delay from isovolumic contraction combined with a strong (relative to the other phenotypes) late-phase delay with diastolic filling managed to capture the characteristic time constants and mitral flow profiles associated with impaired relaxation, while having minimal effects on the aortic pressures and cardiac output.

The second pathology is in passive relaxation, in which the end-diastolic pressure-volume relation increases in nonlinearity and becomes steeper. This is meant to physiologically reflect increased stiffness of the left ventricle. As the main driving mechanism for mitral flow is the atrioventricular pressure gradient, an increase in stiffness allowed the atrioventricular pressure gradient to remain large for the low-volume regime (Fig. 3*D1*), as the volume increased the LV pressure rapidly increased due to the high level of nonlinearity. This rapid equalization (compared with Fig. 3*A1*) of the pressure gradient between the LV and LA created an *E*-wave that is tall and narrow (Fig. 3*D2*). As the ventricular pressure is higher due to increased stiffness before atrial contraction, the contraction of the atrium was not able to fill the heart effectively due to both the increased pressure and increased resistance to expansion, creating a small *A*-wave. It must also be stated that the most important factor in recreating the R phenotype was not the height of the EDPVR but the convexity or nonlinearity. In previous versions of the current cardiac model, the EDPVR was approximated as linear, and increased stiffness was modeled through the increased slope of the EDPVR. This increase in the EDPVR slope would cause a drop in the *E*/*A* ratio. In our nonlinear modeling of EDPVR, we avoid this erroneous *E*/*A* ratio because the stiffness, as derived by the local gradient of the nonlinear EDPVR, was much smaller at low LV volumes right after mitral valve opening than during the atrial contraction, hence most of the expansion occurs right after isovolumic relaxation.

The PN phenotype was replicated by combining the pathologies involved in active relaxation (mainly responsible for IR) and passive relaxation (mainly responsible for R). However, it must be noted that the two main pathologies, namely, increased stiffness and late-phase relaxation, were being combined in their milder form to produce the phenotype. The stiffness for the PN phenotype is larger than that for the IR and the control but smaller than that for the R. The same also applies to the degree of late-phase relaxation in which the PN has a delay that is lower than that of the IR and higher than that of the R. Accordingly, it can be said that the PN phenotype results from the combination of the two principal pathologies underlying IR and R, respectively (increased late-phase delay and increased stiffness), such that their effects on the mitral waveform are cancelled out.

Physiological Mechanisms

As the varying elastance framework used in this article is a phenomenological model that only models the global PV relation, it is difficult to directly relate the pathologies introduced into the diastolic dysfunction models to physiological mechanisms. Increased stiffness of the EDPVR can plausibly be linked to various remodeling processes linked to DD. This includes titin isoform shift and increased collagen content (21). The biphasic delay model is more difficult to physiologically explain. This is because the active relaxation of the heart is an emergent process that encompasses various scales and involves tightly coupled multiphysics phenomena. However, the main clue to follow for the biphasic delay model is that the relaxation rate for the left ventricle is significantly slowed down during early filling. This indicates that the pathological mechanism is possibly dependent on time, calcium levels, myofilament activation, or stretch. The control of diastolic calcium is not well understood (10); however, one possible mechanism currently being investigated is mishandling of calcium during diastole. The dysfunction of ion channels such as sarco(endo)plasmic reticiulum calcium ATPase (SERCA2a), sodium-calcium exchanger (NCX), and ryanodine receptors (RyRs) is currently being implicated in DD (10, 35). One particularly interesting study (42) investigated the different effects that SERCA2a and RyR had on the calcium transients. They found that in the presence of β-adrenergic stimulation, the ryanodine receptor calcium leak induced a biphasic decay of the calcium transient, with an early fast phase and a late slow phase. They also managed to link SERCA2a dysfunction to monophasic delay. A second possible mechanism being investigated is a pathology in myofilament crossbridge dynamics, with the suspected pathology being increased myofilament sensitivity to calcium (10, 35). It is difficult to discover whether the various changes for the cell or sarcomere are causal or correlational with regard to diastolic dysfunction; however, phenomenological studies such as the ones conducted for this article provide hints as to what types of mechanisms should be investigated in the future.

Accordingly, multiscale modeling must be used in the future to investigate how pathologies on the scale of the myocardium affect global organ-level performance. One example of such a model would be the one-fiber model developed by Theo Arts et al. (2) that relates the global PV chamber performance to sarcomere mechanics. The one-fiber model as implemented in contemporary models (1, 22) simulates the sarcomere as a passive elastic element in parallel with an elastic element in series with a contractile element. One important effect that can be investigated is how a change in the passive stiffness with DD would affect the active contraction of the sarcomere, as the

passive stress would resist the contraction of the sarcomeres. Another effect to be investigated is the how the importance of elastic recoil would change throughout the different stages of DD.

It may also seem unintuitive that the progression of diastolic dysfunction from the impaired relaxation stage to the restricted stage necessitates an initial increase and then decrease in late-phase relaxation parameter D_2 (Table 1). However, the following factors must be considered. The interaction between myocardial stiffness and active relaxation is highly complex and not well understood. A recent multiscale modeling study by Campbell et al. (5) demonstrated that cardiac muscle relaxation rate can change significantly with increased nonlinear stiffness of the filaments, as it modulates the rate at which myosin heads move relative to the filament. Thus, the increased stiffness of the PN and R phenotypes can play a modulating role for the D_2 parameter. This is also supported by the finding that one of the main causes of increased stiffness in diastolic dysfunction is titin isoform shift (14). The same computational study also demonstrated that muscle relaxation is sensitive to changes in strain. Furthermore, it is currently understood that relaxation rate is related to the preload and afterload in complex ways (20). Accordingly, these various factors are expected to be relevant to the time course of relaxation during early filling (corresponding to late-phase relaxation) and must be studied further.

Possible Hypotheses

Several testable hypotheses can be derived from the assumptions we used to recreate the various phenotypes. First, it is likely that the central venous pressure increases from IR to PN to R to compensate for the increased stiffness. Second, we expect the stiffness β to be mildly (relative to the control phenotype) increased for patients with a PN phenotype and strongly increased for patients with an R phenotype; we also predict the degree of late-phase delay to follow an equivalent inverse relation. The nature of delayed active relaxation in diastolic dysfunction is not well understood; research must be directed to investigate the causal mechanism of the delay in addition to their timing.

One final hypothesis emerges from the fact that the simulated phenotypes were set up such that their activation functions return to zero by the end of the heart cycle. It is likely that if the heart rate were increased significantly, the ventricle would be unable to completely relax in the case of IR and to a lesser extent in the case of PN, causing increased filling pressures. This was partially explored in a simple 0-D Windkessel-based computational study by Hay et al. (12), in which the effect of ventricular relaxation on pulmonary venous pressure was investigated in tandem with heart rate. Accordingly, if it is true that the degree of delay is the most severe for IR and least severe for R, we would expect the pressure increase during tachycardia for patients with the IR phenotype to be more severe than for patients with the R phenotype.

Central Venous Pressure

Our assumption of increased central venous pressure being the main mechanism behind restoring pressures and volumes is seemingly supported by several studies on HFpEF found in the literature. A previous review by Katz et al. (15) suggests that the central venous pressure might be increased during diastolic dysfunction. This finding is also supported by other studies, such as the study by Burkhoff et al. (4), who collected data on venous pressure with regard to severe end-stage HFpEF and found that patients have a central venous pressure of 12–14 mmHg. In our simulations, we found that increasing the cardiac preload indeed managed to restore the cardiac output through decrease of the ESV and increase of the EDV. The increase in the central venous pressure was propagated throughout the cardiac system and hence led to the increase of also the pressures in the right atrium, right ventricle, pulmonary circulation, and the left atrium. The resulting pulmonary hypertension is consistent with the literature (9) and is possibly linked to further compensatory mechanisms.

It must be noted that here we investigated solely the effect of venous return on the restoration of the cardiac output and on the disease phenotype. However, a change in the function of the atria or right ventricle may also regulate the cardiac output; hence, the cardiac output compensation may not need be completely modulated by just an increase in venous return. In fact, it is expected that the cardiovascular system uses multiple remodeling methods to adjust itself, the exploration of which might provide further insight into the disease mechanisms.

Model Limitations

The largest limitation of the model is that it is currently an open-loop model, whereby pressure changes in the systemic blood vessels do not propagate forward to affect the right atrium. Using a closed-loop model would provide a better estimate of the venous pressure and allow for the control of the venous pressure through changing the systemic vein parameters. The pulmonary model is currently a simplified 0-D lumped parameter model, and a proper investigation of dyspnea would require a more complex pulmonary model to analyze the pulmonary vessel volume change with diastolic dysfunction. Furthermore, there is some literature detailing how the pulmonary vein flow can be used to diagnose diastolic dysfunction, which could possibly be captured by a more complex pulmonary model.

It must also be noted that HFpEF is linked to structural and functional changes in the right ventricle (24, 39, 46) and left atrium (8, 30, 44). However, for the purposes of this article, the effects of these changes were not systematically investigated and are left to future studies. Furthermore, to our knowledge, there are very little data available on the three main parameters investigated in this study. In fact, one of the main arguments of this article is that the traditional way of measuring active relaxation through the time constant of relaxation is insufficient for characterizing DD. Clinically, the active relaxation of the cardiac chamber is taken to be represented mainly by the pressure drop during the isovolumic phase. However, what the biphasic delay model implies is that the time course of active relaxation has a critical causal role in dictating mitral flow hemodynamics. Accordingly, from this study, it follows that clinicians should focus more on understanding and measuring the active relaxation pathologies involved in both early phase (isovolumic) and late-phase (diastolic) relaxation.

Another issue is the inability of the model to fully capture the correct progression of the IVRT. According to the literature, the IVRT for the R phenotype should be lower than the

control value of 65 ms, but instead it was calculated to be 85 ms. This is because the changes in both time constant and IVRT are proportionally linked to the same parameter D_1; the choice of D_1 to fit the increased time constants for the DD stages dictates a similar progression for the IVRTs. This may be because there are little high-quality data relating to the time constant of the R phenotype; it could be possible that more precise clinical studies on the R stage of DD show that the time constant is not as increased as for the other stages, in which case, the subsequent tuning of the simulation would likely produce an IVRT that matches the expected value.

Conclusions

The main purpose of this computational model was to replicate in a biomechanically and hemodynamically relevant manner, the main pathological phenotypes of diastolic dysfunction. This was done by isolating the pathological diastolic behavior into three parameters—the biphasic delay model is controlled by two parameters for active relaxation (early and late-phase delays) and one parameter for passive relaxation (stiffness). It was found that a combination of increasing both early and late-phase delays can replicate the hemodynamic parameters associated with impaired relaxation. An increase in stiffness and a decrease in late-phase delay compared with the impaired relaxation case managed to recreate the progression to pseudo-normal, with the restrictive phenotype being the result of strongly increased stiffness and little delay. However, it must be noted that changing only the diastolic portion of heart behavior by itself tends to significantly decrease the maximum left ventricular pressure, end-diastolic and end-systolic volumes, and cardiac output. These parameters are either normal or slightly abnormal in people with DD. Accordingly, it stands to reason that patients with any form of DD will correspondingly have different cardiac and systemic properties to compensate for a pathological diastolic phase. It was found that the most influential possible mechanism for the restoration of the cardiac output was an increase in the venous pressure. From this holistic replication of DD, the biomechanics of the pathology is further elucidated. Furthermore, several hypotheses were produced and research directions were suggested for future research.

DISCLAIMERS

All authors approved the final version of the manuscript and agree to be accountable for all aspects of the work in ensuring that questions related to the accuracy or integrity of any part of the work are appropriately investigated and resolved.

DISCLOSURES

No conflicts of interest, financial or otherwise, are declared by the authors.

AUTHOR CONTRIBUTIONS

K.K., S.P., D.A., and N.S. conceived and designed research; K.K. and Q.M. performed experiments; K.K. analyzed data; K.K., S.P., G.R., V.B., H.M., D.A., and N.S. interpreted results of experiments; K.K. and S.P. prepared figures; K.K. and S.P. drafted manuscript; K.K., S.P., Q.M., G.R., V.B., H.M., D.A., and N.S. edited and revised manuscript; K.K., S.P., Q.M., G.R., V.B., H.M., D.A., and N.S. approved final version of manuscript.

REFERENCES

1. **Arts T, Delhaas T, Bovendeerd P, Verbeek X, Prinzen FW.** Adaptation to mechanical load determines shape and properties of heart and circulation: the CircAdapt model. *Am J Physiol Heart Circ Physiol* 288: H1943–H1954, 2005. doi:10.1152/ajpheart.00444.2004.
2. **Arts T, Reneman RS, Veenstra PC.** A model of the mechanics of the left ventricle. *Ann Biomed Eng* 7: 299–318, 1979. doi:10.1007/BF02364118.
3. **Borlaug BA, Lam CS, Roger VL, Rodeheffer RJ, Redfield MM.** Contractility and ventricular systolic stiffening in hypertensive heart disease insights into the pathogenesis of heart failure with preserved ejection fraction. *J Am Coll Cardiol* 54: 410–418, 2009. doi:10.1016/j.jacc.2009.05.013.
4. **Burkhoff D, Maurer MS, Joseph SM, Rogers JG, Birati EY, Rame JE, Shah SJ.** Left atrial decompression pump for severe heart failure with preserved ejection fraction: theoretical and clinical considerations. *JACC Heart Fail* 3: 275–282, 2015. doi:10.1016/j.jchf.2014.10.011.
5. **Campbell KS.** Compliance accelerates relaxation in muscle by allowing myosin heads to move relative to actin. *Biophys J* 110: 661–668, 2016. doi:10.1016/j.bpj.2015.12.024.
6. **Christensen NL, Dahl JS, Carter-Storch R, Jensen K, Pecini R, Steffensen FH, Søndergaard EV, Videbæk LM, Møller JE.** Association between left ventricular diastolic function and right ventricular function and morphology in asymptomatic aortic stenosis. *PLoS One* 14: e0215364, 2019. doi:10.1371/journal.pone.0215364.
7. **Danielsen M.** *Modeling of feedback mechanisms which control the heart function in a view to an implementation in cardiovascular models* (PhD thesis). Denmark: Roskilda University, 1998.
8. **Danzmann LC, Bodanese LC, Köhler I, Torres MR.** Left atrioventricular remodeling in the assessment of the left ventricle diastolic function in patients with heart failure: a review of the currently studied echocardiographic variables. *Cardiovasc Ultrasound* 6: 56, 2008. doi:10.1186/1476-7120-6-56.
9. **de Jesus Perez VA, Haddad F, Zamanian RT.** Diagnosis and management of pulmonary hypertension associated with left ventricular diastolic dysfunction. *Pulm Circ* 2: 163–169, 2012. doi:10.4103/2045-8932.97598.
10. **Eisner DA, Caldwell JL, Trafford AW, Hutchings DC.** The control of diastolic calcium in the heart: basic mechanisms and functional implications. *Circ Res* 126: 395–412, 2020. doi:10.1161/CIRCRESAHA.119.315891.
11. **Galderisi M.** Diastolic dysfunction and diastolic heart failure: diagnostic, prognostic and therapeutic aspects. *Cardiovasc Ultrasound* 3: 9, 2005. doi:10.1186/1476-7120-3-9.
12. **Hay I, Rich J, Ferber P, Burkhoff D, Maurer MS.** Role of impaired myocardial relaxation in the production of elevated left ventricular filling pressure. *Am J Physiol Heart Circ Physiol* 288: H1203–H1208, 2005. doi:10.1152/ajpheart.00681.2004.
13. **Hsiao SH, Lin KL, Chiou KR.** Comparison of left atrial volume parameters in detecting left ventricular diastolic dysfunction versus tissue Doppler recordings. *Am J Cardiol* 109: 748–755, 2012. doi:10.1016/j.amjcard.2011.10.040.
14. **Jeong EM, Dudley SC Jr.** Diastolic dysfunction. *Circ J* 79: 470–477, 2015. doi:10.1253/circj.CJ-15-0064.
15. **Katz AM, Rolett EL.** Heart failure: when form fails to follow function. *Eur Heart J* 37: 449–454, 2016. doi:10.1093/eurheartj/ehv548.
16. **Kawaguchi M, Hay I, Fetics B, Kass DA.** Combined ventricular systolic and arterial stiffening in patients with heart failure and preserved ejection fraction: implications for systolic and diastolic reserve limitations. *Circulation* 107: 714–720, 2003. doi:10.1161/01.CIR.0000048123.22359.A0.
17. **Kuznetsova T, Herbots L, López B, Jin Y, Richart T, Thijs L, González A, Herregods M-C, Fagard RH, Díez J, Staessen JA.** Prevalence of left ventricular diastolic dysfunction in a general population. *Circ Heart Fail* 2: 105–112, 2009. doi:10.1161/CIRCHEARTFAILURE.108.822627.
18. **Lam CS, Donal E, Kraigher-Krainer E, Vasan RS.** Epidemiology and clinical course of heart failure with preserved ejection fraction. *Eur J Heart Fail* 13: 18–28, 2011. doi:10.1093/eurjhf/hfq121.
19. **Lam CS, Roger VL, Rodeheffer RJ, Bursi F, Borlaug BA, Ommen SR, Kass DA, Redfield MM.** Cardiac structure and ventricular-vascular function in persons with heart failure and preserved ejection fraction from Olmsted County, Minnesota. *Circulation* 115: 1982–1990, 2007. doi:10.1161/CIRCULATIONAHA.106.659763.
20. **Leite-Moreira AF, Correia-Pinto J.** Load as an acute determinant of end-diastolic pressure-volume relation. *Am J Physiol Heart Circ Physiol* 280: H51–H59, 2001. doi:10.1152/ajpheart.2001.280.1.H51.
21. **LeWinter MM, Meyer M.** Mechanisms of diastolic dysfunction in heart failure with a preserved ejection fraction: If it's not one thing it's another. *Circ Heart Fail* 6: 1112–1115, 2013. doi:10.1161/CIRCHEARTFAILURE.113.000825.

22. **Lumens J, Delhaas T, Kirn B, Arts T.** Three-wall segment (TriSeg) model describing mechanics and hemodynamics of ventricular interaction. *Ann Biomed Eng* 37: 2234–2255, 2009. doi:10.1007/s10439-009-9774-2.
23. **Luo C, Ramachandran D, Ware DL, Ma TS, Clark JW Jr.** Modeling left ventricular diastolic dysfunction: classification and key indicators. *Theor Biol Med Model* 8: 14, 2011. doi:10.1186/1742-4682-8-14.
24. **Melenovsky V, Hwang SJ, Lin G, Redfield MM, Borlaug BA.** Right heart dysfunction in heart failure with preserved ejection fraction. *Eur Heart J* 35: 3452–3462, 2014. doi:10.1093/eurheartj/ehu193.
25. **Mossahebi S, Zhu S, Kovács SJ.** Fractionating E-wave deceleration time into its stiffness and relaxation components distinguishes pseudonormal from normal filling. *Circ Cardiovasc Imaging* 8: e002177, 2015. doi:10.1161/CIRCIMAGING.114.002177.
26. **Mottram PM, Marwick TH.** Assessment of diastolic function: what the general cardiologist needs to know. *Heart* 91: 681–695, 2005. doi:10.1136/hrt.2003.029413.
27. **Mynard JP, Davidson MR, Penny DJ, Smolich JJ.** A simple, versatile valve model for use in lumped parameter and one-dimensional cardiovascular models. *Int J Numer Method Biomed Eng* 28: 626–641, 2012. doi:10.1002/cnm.1466.
28. **Mynard JP, Smolich JJ.** One-dimensional haemodynamic modeling and wave dynamics in the entire adult circulation. *Ann Biomed Eng* 43: 1443–1460, 2015. doi:10.1007/s10439-015-1313-8.
29. **Nagueh SF, Smiseth OA, Appleton CP, Byrd BF 3rd, Dokainish H, Edvardsen T, Flachskampf FA, Gillebert TC, Klein AL, Lancellotti P, Marino P, Oh JK, Popescu BA, Waggoner AD.** Recommendations for the evaluation of left ventricular diastolic function by echocardiography: an update from the American Society of Echocardiography and the European Association of Cardiovascular Imaging. *J Am Soc Echocardiogr* 29: 277–314, 2016. doi:10.1016/j.echo.2016.01.011.
30. **Nedios S, Koutalas E, Sommer P, Arya A, Rolf S, Husser D, Bollmann A, Hindricks G, Breithardt OA.** Asymmetrical left atrial remodelling in atrial fibrillation: relation with diastolic dysfunction and long-term ablation outcomes. *Eurospace* 19: 1463–1469, 2017. doi:10.1093/europace/euw225.
31. **Pagoulatou S, Stergiopulos N.** Evolution of aortic pressure during normal ageing: A model-based study. *PLoS One* 12: e0182173, 2017. doi:10.1371/journal.pone.0182173.
32. **Pagoulatou SZ, Stergiopulos N.** Estimating left ventricular elastance from aortic flow waveform, ventricular ejection fraction, and brachial pressure: an in silico study. *Ann Biomed Eng* 46: 1722–1735, 2018. doi:10.1007/s10439-018-2072-0.
33. **Paulus WJ, Tschope C, Sanderson JE, Rusconi C, Flachskampf FA, Rademakers FE, Marino P, Smiseth OA, Keulenaer GD, Leite-Moreira AF, Borbely A, Edes I, Handoko ML, Heymans S, Pezzali N, Pieske B, Dickstein K, Fraser AG, Brutsaert DL.** How to diagnose diastolic heart failure: a consensus statement on the diagnosis of heart failure with normal left ventricular ejection fraction by the Heart Failure and Echocardiography Associations of the European Society of Cardiology. *Eur Heart J* 28: 2539–2550, 2007. doi:10.1093/eurheartj/ehm037.
34. **Penicka M, Bartunek J, Trakalova H, Hrabakova H, Maruskova M, Karasek J, Kocka V.** Heart failure with preserved ejection fraction in outpatients with unexplained dyspnea: a pressure-volume loop analysis. *J Am Coll Cardiol* 55: 1701–1710, 2010. doi:10.1016/j.jacc.2009.11.076.
35. **Periasamy M, Janssen PM.** Molecular basis of diastolic dysfunction. *Heart Fail Clin* 4: 13–21, 2008. doi:10.1016/j.hfc.2007.10.007.
36. **Reymond P, Bohraus Y, Perren F, Lazeyras F, Stergiopulos N.** Validation of a patient-specific one-dimensional model of the systemic arterial tree. *Am J Physiol Heart Circ Physiol* 301: H1173–H1182, 2011. doi:10.1152/ajpheart.00821.2010.
37. **Reymond P, Merenda F, Perren F, Rüfenacht D, Stergiopulos N.** Validation of a one-dimensional model of the systemic arterial tree. *Am J Physiol Heart Circ Physiol* 297: H208–H222, 2009. doi:10.1152/ajpheart.00037.2009.
38. **Reymond P, Westerhof N, Stergiopulos N.** Systolic hypertension mechanisms: effect of global and local proximal aorta stiffening on pulse pressure. *Ann Biomed Eng* 40: 742–749, 2012. doi:10.1007/s10439-011-0443-x.
39. **Rommel KP, von Roeder M, Oberueck C, Latuscynski K, Besler C, Blazek S, Stiermaier T, Fengler K, Adams V, Sandri M, Linke A, Schuler G, Thiele H, Lurz P.** Load-independent systolic and diastolic right ventricular function in heart failure with preserved ejection fraction as assessed by resting and handgrip exercise pressure-volume loops. *Circ Heart Fail* 11: e004121, 2018. doi:10.1161/CIRCHEARTFAILURE.117.004121.
40. **Sagawa K.** The end-systolic pressure-volume relation of the ventricle: definition, modifications and clinical use. *Circulation* 63: 1223–1227, 1981. doi:10.1161/01.CIR.63.6.1223.
41. **Sagawa K, Suga H, Shoukas AA, Bakalar KM.** End-systolic pressure/volume ratio: a new index of ventricular contractility. *Am J Cardiol* 40: 748–753, 1977. doi:10.1016/0002-9149(77)90192-8.
42. **Sankaranarayanan R, Li Y, Greensmith DJ, Eisner DA, Venetucci L.** Biphasic decay of the Ca transient results from increased sarcoplasmic reticulum Ca leak. *J Physiol* 594: 611–623, 2016. doi:10.1113/JP271473.
43. **Sato K, Grant AD, Negishi K, Cremer PC, Negishi T, Kumar A, Collier P, Kapadia SR, Grimm RA, Desai MY, Griffin BP, Popović ZB.** Reliability of updated left ventricular diastolic function recommendations in predicting elevated left ventricular filling pressure and prognosis. *Am Heart J* 189: 28–39, 2017. doi:10.1016/j.ahj.2017.03.022.
44. **Teo SG, Yang H, Chai P, Yeo TC.** Impact of left ventricular diastolic dysfunction on left atrial volume and function: a volumetric analysis. *Eur J Echocardiogr* 11: 38–43, 2010. doi:10.1093/ejechocard/jep153.
45. **Tsao CW, Lyass A, Enserro D, Larson MG, Ho JE, Kizer JR, Gottdiener JS, Psaty BM, Vasan RS.** Temporal trends in the incidence of and mortality associated with heart failure with preserved and reduced ejection fraction. *JACC Heart Fail* 6: 678–685, 2018. doi:10.1016/j.jchf.2018.03.006.
46. **von Roeder M, Kowallick JT, Rommel K-P, Blazek S, Besler C, Fengler K, Lotz J, Hasenfuß G, Lücke C, Gutberlet M, Thiele H, Schuster A, Lurz P.** Right atrial–right ventricular coupling in heart failure with preserved ejection fraction. *Clin Res Cardiol* 109: 54–66, 2020. doi:10.1007/s00392-019-01484-0.
47. **Wang J, Khoury DS, Yue Y, Torre-Amione G, Nagueh SF.** Preserved left ventricular twist and circumferential deformation, but depressed longitudinal and radial deformation in patients with diastolic heart failure. *Eur Heart J* 29: 1283–1289, 2008. doi:10.1093/eurheartj/ehn141.
48. **Weber T, Auer J, O'Rourke MF, Punzengruber C, Kvas E, Eber B.** Prolonged mechanical systole and increased arterial wave reflections in diastolic dysfunction. *Heart* 92: 1616–1622, 2006. doi:10.1136/hrt.2005.084145.
49. **Yoon S, Eom GH.** Heart failure with preserved ejection fraction: present status and future directions. *Exp Mol Med* 51: 1–9, 2019. doi:10.1038/s12276-019-0323-2.
50. **Zile MR, Baicu CF, Gaasch WH.** Diastolic heart failure–abnormalities in active relaxation and passive stiffness of the left ventricle. *N Engl J Med* 350:1953–1959, 2004. doi:10.1056/NEJMoa032566.
51. **Zile MR, Brutsaert DL.** New concepts in diastolic dysfunction and diastolic heart failure: Part I: diagnosis, prognosis, and measurements of diastolic function. *Circulation* 105: 1387–1393, 2002. doi:10.1161/hc1102.105289.
52. **Zile MR, Gaasch WH, Carroll JD, Feldman MD, Aurigemma GP, Schaer GL, Ghali JK, Liebson PR.** Heart failure with a normal ejection fraction: is measurement of diastolic function necessary to make the diagnosis of diastolic heart failure? *Circulation* 104: 779–782, 2001. doi:10.1161/hc3201.094226.